atmosphere

Article

Decomposition of Trend and Interdecadal Variation of Evaporation over the Tropical Indian Ocean in ERA5

Bicheng Huang [1,2], Tao Su [1], Zengping Zhang [1], Yongping Wu [1] and Guolin Feng [1,3,4,*]

[1] College of Physical Science and Technology, Yangzhou University, Yangzhou 225005, China; huangbch18@lzu.edu.cn (B.H.); taosu@yzu.edu.cn (T.S.); zpzhang@yzu.edu.cn (Z.Z.); ypwu@yzu.edu.cn (Y.W.)
[2] College of Atmospheric Sciences, Lanzhou University, Lanzhou 730000, China
[3] Laboratory for Climate Studies, China Meteorological Administration, Beijing 100081, China
[4] Southern Marine Science and Engineering Guangdong Laboratory, Zhuhai 511458, China
* Correspondence: fenggl@cma.gov.cn

Abstract: Based on ERA5 from 1980 to 2018, we compare and analyze the trend and interdecadal variation of evaporation anomalies over the tropical Indian Ocean by the evaporation decomposition method. This method mainly decomposes the evaporation anomalies into the Newtonian cooling, stability, relative humidity, wind speed, and transfer coefficient terms. The annual mean evaporation anomalies show an increasing trend (0.083 mm/d/decade). The Newtonian cooling term (0.026 mm/d/decade), the relative humidity term (0.032 mm/d/decade), and the wind speed term (0.026 mm/d/decade) play a major role in the increasing trend. The interdecadal variation of evaporation anomalies shows decreases in the 1980s and after the early 2000s, and an increase in the 1990s. The decreased evaporation anomalies in the 1980s are affected by the transfer coefficient term, which is associated with the North Atlantic Oscillation (NAO). The increased evaporation anomalies in the 1990s and the decreased evaporation anomalies since the early 2000s are largely controlled by the wind speed term, which are dominated by the Atlantic Multidecadal Oscillation (AMO). The Pacific Decadal Oscillation (PDO) may have important impacts on the interdecadal increase of evaporation anomalies by affecting the wind speed in the 1990s.

Keywords: tropical Indian Ocean evaporation; trend and interdecadal variation; evaporation decomposition; climate modes

Citation: Huang, B.; Su, T.; Zhang, Z.; Wu, Y.; Feng, G. Decomposition of Trend and Interdecadal Variation of Evaporation over the Tropical Indian Ocean in ERA5. *Atmosphere* **2022**, *13*, 496. https://doi.org/10.3390/atmos13030496

Academic Editor: Anita Drumond

Received: 12 February 2022
Accepted: 16 March 2022
Published: 19 March 2022

1. Introduction

Ocean evaporation is important for the exchange of heat and moisture between the atmosphere and ocean [1–3]. The changes in ocean evaporation can affect the sea surface temperature (SST) by atmospheric feedback and the freshwater flux (evaporation minus precipitation) and atmospheric circulation by energy exchanges [4–6]. During recent decades the tropical Indian Ocean SST has experienced rapid warming, with enhanced evaporation [7–9]. Therefore, understanding the tropical Indian Ocean evaporation variability is essential for the water and energy budget and the complex interaction between the atmosphere and ocean [10].

Although many studies pointed out that the magnitude of ocean evaporation differs considerably in different evaporation datasets [11–13], the ocean evaporation displays a significant increasing trend and has similar interdecadal variation [14–16]. Due to the development of modern observations and model simulations, the recently released fifth generation of European Centre for Medium-Range Weather Forecasts (ECMWF) reanalysis (ERA5) shows the most reliable estimate in the surface flux over the tropical Indian Ocean [17].

The ocean evaporation is estimated using similar aerodynamic bulk formulae [18,19], which is significantly affected by different factors, such as SST, surface air temperature, near-surface relative humidity, and near-surface wind speed [20]. Lorenz et al. [21] found that the increased relative humidity mainly contributes to the reduction in the evaporation increase below the Clausius–Clapeyron rate. The increasing trend of evaporation over the tropical Pacific is closely related to the SST warming and the enhanced wind speed [15]. The interdecadal trends of global ocean evaporation are affected by the air-sea humidity difference and the wind speed [22]. The enhanced near-surface wind speed leads to negative SST anomalies by the enhanced evaporation, popularly known as wind-evaporation-SST (WES) feedback [23]. Therefore, it is essential to analyze and understand the contribution of these factors to ocean evaporation.

The sensitivities of ocean evaporation to the factors have been analyzed in previous studies [10,24]. However, these studies were restricted to the influence of the factors on evaporation. In this study, we not only quantify the influence of the factors on the evaporation, but also examine the long-term trend and interdecadal variation of evaporation. Recent studies indicated that the evaporation decomposition method can quantify the contribution of the factors controlling ocean evaporation [25,26]. The increased relative humidity, increased air-sea temperature difference, and decreased wind speed reduce the increase in the global ocean [19] and tropical Indian Ocean evaporation [8] to 2%/K in the model simulations. The wind speed plays a dominant role in the increased evaporation, and moisture difference contributes to the decreased evaporation over the quasi-global oceans on the interdecadal scale [25]. Therefore, this study focuses on the trend and interdecadal variation of the annual and seasonal mean evaporation anomaly for the period 1980–2018 over the tropical Indian Ocean using ERA5. The impacts of the main factors (SST, sea-air temperature difference, relative humidity, wind speed, and transfer coefficient) on the evaporation anomaly are also investigated by the evaporation decomposition method, and the related climate variations are discussed.

2. Data and Methods

2.1. Data

ERA5 is the latest reanalysis produced by ECMWF from 1979 to present with 0.25° × 0.25° horizontal resolution [27]. The variables, including evaporation, surface air temperature, surface dew point temperature, and surface wind speed, were used in this study. The monthly SST dataset is derived from the National Oceanic and Atmospheric Administration (NOAA) Extended Reconstructed SST version 5 (ERSSTv5) on a horizontal resolution of 2° × 2° [28]. In this study, we focused on the spatial mean of the tropical Indian Ocean (40° E–120° E, 30° S–30° N) during the period 1980–2018 (Figure 1). For a better match of the spatial domain used to calculate area-averaged values, the ERA5 dataset was interpolated into a 2° × 2° grid using bilinear interpolation. In addition, the North Atlantic Oscillation (NAO), Pacific Decadal Oscillation (PDO), and Atlantic Multidecadal Oscillation (AMO) were downloaded from Climate Explorer and used to analyze the related climate variability.

2.2. Evaporation Decomposition Method

We used a diagnostic partitioning of the bulk aerodynamic formulation for evaporation following Richter and Xie [19]:

$$\mathrm{EVP} = \mathrm{C_E}\rho_a \mathrm{U}[\mathrm{q_s}(\mathrm{SST}) - \mathrm{RH} \times \mathrm{q_s}(\mathrm{SST} + \mathrm{S})] \quad (1)$$

where $\mathrm{C_E}$ is the transfer coefficient and ρ_a, U, and RH are the surface air density, surface wind speed, and surface relative humidity, respectively. $\mathrm{S} = \mathrm{SAT} - \mathrm{SST}$ is the difference between the surface air temperature (SAT) and SST, representing the surface stability. $\mathrm{q_s}(\mathrm{SST})$ is the saturated specific humidity. $\mathrm{RH} \times \mathrm{q_s}(\mathrm{SST} + \mathrm{S})$ is the surface-specific humidity. To estimate the contributions of each factor to evaporation, the evaporation anomalies (EVP') were decomposed following previous studies [25,26]:

$$\mathrm{EVP}' = \frac{\partial \mathrm{EVP}}{\partial \mathrm{SST}}\mathrm{SST}' + \frac{\partial \mathrm{EVP}}{\partial \mathrm{S}}\mathrm{S}' + \frac{\partial \mathrm{EVP}}{\partial \mathrm{RH}}\mathrm{RH}' + \frac{\partial \mathrm{EVP}}{\partial \mathrm{U}}\mathrm{U}' + \frac{\partial \mathrm{EVP}}{\partial \mathrm{C_E}}\mathrm{C_E}' + \mathrm{RES} \tag{2}$$

where the partial derivatives are calculated from monthly climatology, representing the sensitivity of evaporation to each factor. The prime denotes a departure from monthly climatology, which, in our case, is based on the period 1980–2018. The right side of the equation represents the Newtonian cooling term (NC), surface stability term (S*), relative humidity term (RH*), wind speed term (U*), transfer coefficient term (C_E*, which is calculated by dividing the evaporation by $\rho_a U[q_s(\mathrm{SST}) - \mathrm{RH} \times q_s(\mathrm{SST}+\mathrm{S})]$), and residual term (RES), respectively. This symbol (*) is used to distinguish surface stability term (S*) from surface stability (S).

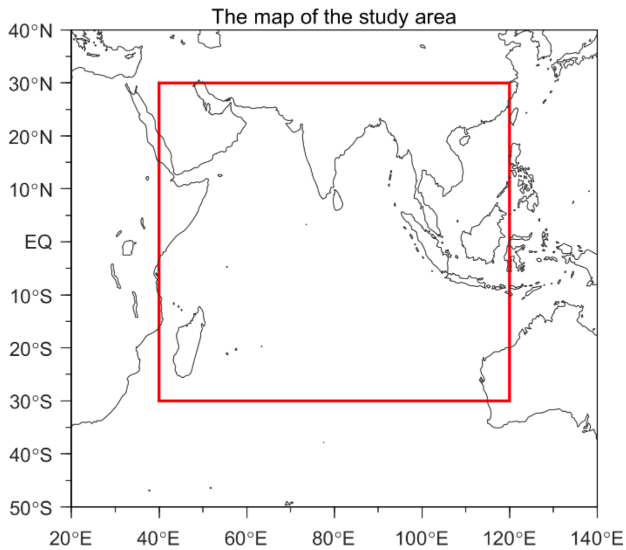

Figure 1. Map of the study area. The red rectangle indicates the tropical Indian Ocean (40° E–120° E, 30° S–30° N).

2.3. Statistical Methods

The trend of evaporation and its main factors for the period 1980–2018 were calculated by the linear ordinary least squares method. To extract the interdecadal variation (IDV), all variables were first detrended by removing the linear trend, and we performed the 9-year running mean on the detrended annual mean (the average values in January–December, namely Year) evaporation anomalies and seasonal mean evaporation anomalies from spring to winter (the average values in March–April–May, June–July–August, September–October–November, and December–January–February, namely MAM, JJA, SON, and DJF) over the tropical Indian Ocean and their main factors. The statistical significances of correlation coefficients and trends were based on a two-tailed Student's *t*-test. In this study, to keep the same number of years of data used to calculate the averages, we used 38 years (1981–2018) of data in Year, MAM, JJA, and SON and 38 years (1981–2018) of data in DJF. To consider the influence of 9-year running mean on degrees of freedom, the effective number of degrees of freedom was calculated following previous studies [29,30]:

$$\frac{1}{\mathrm{N^{eff}}} \approx \frac{1}{\mathrm{N}} + \frac{2}{\mathrm{N}}\sum_{\mathrm{j}=1}^{\mathrm{N}} \frac{\mathrm{N}-\mathrm{j}}{\mathrm{N}}\rho_{\mathrm{XX}}(\mathrm{j})\rho_{\mathrm{YY}}(\mathrm{j}) \tag{3}$$

where N is the sample size and $\rho_{XX}(j)$ and $\rho_{YY}(j)$ are the autocorrelations of two sampled time series X and Y at time lag j, respectively.

3. Results

3.1. Trend of Evaporation over the Tropical Indian Ocean

Figure 2 shows the linear trend and interdecadal variation of annual mean EVP′ over the tropical Indian Ocean in ERA5. An increasing EVP′ was observed with a significant linear trend of 0.085 mm/d/decade with a 99% confidence level. A clear interdecadal variation was observed, showing a negative EVP′ from the 1980s to the mid-1990s and from 2010 onwards and positive EVP′ from the mid-1990s to the 2000s. The results are consistent with previous studies [22,31]. We further investigated the main factors affecting the increasing trend of EVP′ by the evaporation decomposition method. Table 1 shows the trends of annual and seasonal mean EVP′ and the related decomposition terms. From the annual mean EVP′, the significant trends of NC, RH*, and U* were 0.026, 0.031, and 0.026 mm/d/decade, respectively. These results indicate that the NC, U*, and RH* were the major contributors to the increasing trend of EVP′, being the latter slightly more important.

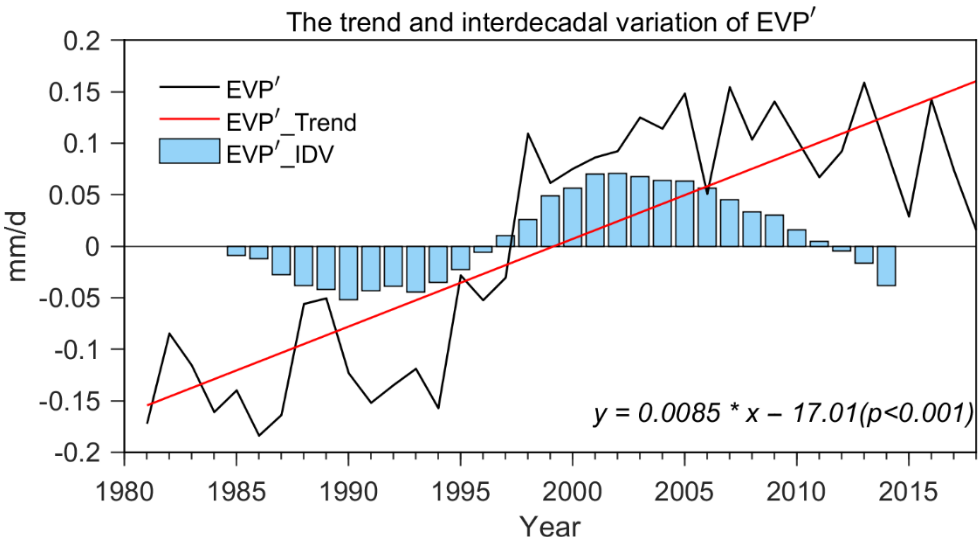

Figure 2. Time series of annual mean evaporation anomalies (EVP′; black solid curve; unit: mm/d) over the tropical Indian Ocean, linear trend (EVP′ _Trend; red solid curve; unit: mm/d/year) and interdecadal variation (EVP′ _IDV; blue bars; unit: mm/d) of annual mean evaporation anomalies over the tropical Indian Ocean.

Table 1. The trends of annual and seasonal mean evaporation anomalies and the decomposition terms. Unit: mm/d/decade.

	EVP′	NC	S*	RH*	U*	C_E*
Year	***0.085***	***0.026***	−0.004	***0.031***	***0.026***	0.001
MAM	***0.098***	***0.022***	0	***0.035***	0.034	0.004
JJA	***0.081***	***0.03***	0.003	***0.036***	0.01	0.002
SON	***0.078***	***0.027***	***−0.014***	***0.021***	**0.029**	0.013
DJF	***0.086***	***0.025***	−0.006	***0.032***	**0.033**	0.001

Note: the values in bold font and bold italic font are significant with the 95 and 99% confidence level, respectively.

Similar to the annual mean EVP′, the NC, RH*, and U* play major roles in the increasing trend of seasonal mean EVP′ (Table 1). The EVP′ increase reached its maximum (0.098 mm/d/decade) in MAM, which may be affected by the magnitude of the U* trend. The EVP′ increase showed a minimum (0.078 mm/d/decade) in SON, which is affected by the magnitude of the RH* trend and a negative S* trend. In JJA, the increasing trend of EVP′ was mainly due to a positive trend in NC associated with an SST warming and a positive trend in RH*. The positive U* trend was not significant with a 95% confidence level in MAM and JJA. Although the positive U* trends had a large magnitude in SON and DJF, they were significant with a 95% confidence level and not significant with a 99% confidence level. Therefore, the upward trends of the seasonal mean EVP′ were mainly affected by the NC, U*, and RH*, and their magnitude was significantly affected by the S*, especially in SON. Under greenhouse warming, the increased downward longwave radiation warmed the tropical Indian Ocean, leading to SST warming and evaporation increasing [8]. The increased saturated specific humidity in global warming could tend to reduce relative humidity, which may further promote the increase in evaporation [16,32]. The wind speed showed an increasing trend over the past two decades, which was likely associated with the increasing trend of evaporation [14,33,34].

3.2. Interdecadal Variation of Evaporation over the Tropical Indian Ocean

Next, we investigated the dominant factors of interdecadal variation of EVP′ over the tropical Indian Ocean. Figure 3 shows the IDV of the annual mean EVP′ and the related decomposition terms. The IDV of the EVP′ showed a small downward trend in the 1980s, an upward trend from the 1990s to the early 2000s, and a downward trend from the early 2000s onwards. Note that the RES is small and bears little resemblance to the IDV of EVP′, suggesting that the evaporation decomposition method has captured the main features in the IDV of the EVP′. The IDV of the U* increased from the 1980s to the early 2000s and decreased since about 2005, similar to the results of Yu [22]. The correlation coefficient between the IDV of U* and EVP′ was 0.81 with the 95% confidence level. The IDV of C_E* decreased in the 1980s, corresponding to the downward trend of the IDV of EVP′ (Figure 3b). The IDV of C_E* showed high correlation with the IDV of EVP′ (0.78, above the 95% confidence level), suggesting that C_E has an important influence on the IDV of EVP′. Although the IDV of RH*, similar to the IDV of EVP′, the correlation between the IDV of RH* and EVP′ was not significant with the 95% confidence level (the effective number of degrees of freedom was 5). The results indicate that the U* and C_E* play a major role in the IDV of EVP′. The C_E* contributed to the IDV of EVP′ in the 1980s and the U* contributed to the IDV of EVP′ after the late 1990s.

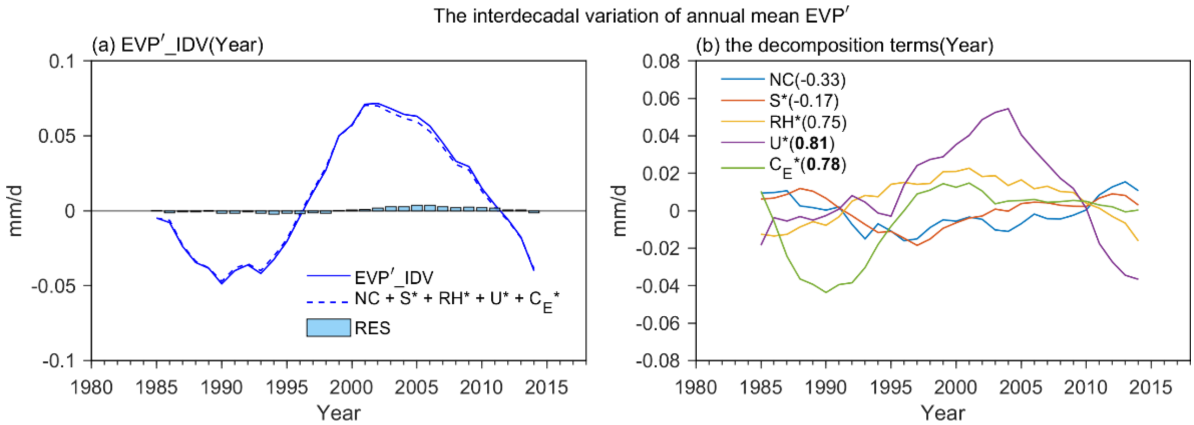

Figure 3. (**a**) Time series of the interdecadal variation of annual mean EVP′ (blue solid line), the sum of the interdecadal variations of Newtonian cooling term (NC), surface stability term (S*), relative humidity term (RH*), wind speed term (U*), exchange coefficient term (C_E*) (blue dashed line), and residual term (RES, blue bars) over the tropical Indian Ocean. (**b**) The interdecadal variation of annual mean NC, S*, RH*, U*, and C_E*. The correlation coefficients between the interdecadal variations of EVP′ and the decomposition terms are written in brackets (correlations significant with the 95% confidence level are in bold). All units are in mm/d.

Furthermore, the IDV of EVP′ and the related decomposition terms from MAM to DJF are shown in Figure 4. The IDVs of MAM and SON EVP′ were similar to the IDV of the annual mean EVP′. The IDV of EVP′ featured an upward trend from the 1980s to the early 2000s and the downward trend from the early 2000s onwards in JJA. The IDV of DJF EVP′

showed a downward trend in the 1980s and an upward trend in the 1990s. Compared with the IDV of the annual mean EVP′, the IDV of C_E* showed low correlation with the IDV of EVP′ in MAM, and the IDV of RH* also had a significant correlation (0.86) with the IDV of EVP′ in JJA. The correlation between the IDV of RH* and EVP′ exceeded that of the IDV of U* and EVP′ in JJA. The IDV of C_E* had a high correlation (0.9) with the IDV of EVP′ in DJF with a 95% confidence level, suggesting that the C_E* contributed largely to the IDV of EVP′ in DJF. Overall, the IDV of EVP′ was not consistent in different seasons. The U* played an important role in the IDV of EVP′ in all seasons, the RH* contributed to the IDV of EVP′ in JJA, and the C_E* exerted an important influence on the IDV of EVP′ in JJA, SON, and DJF.

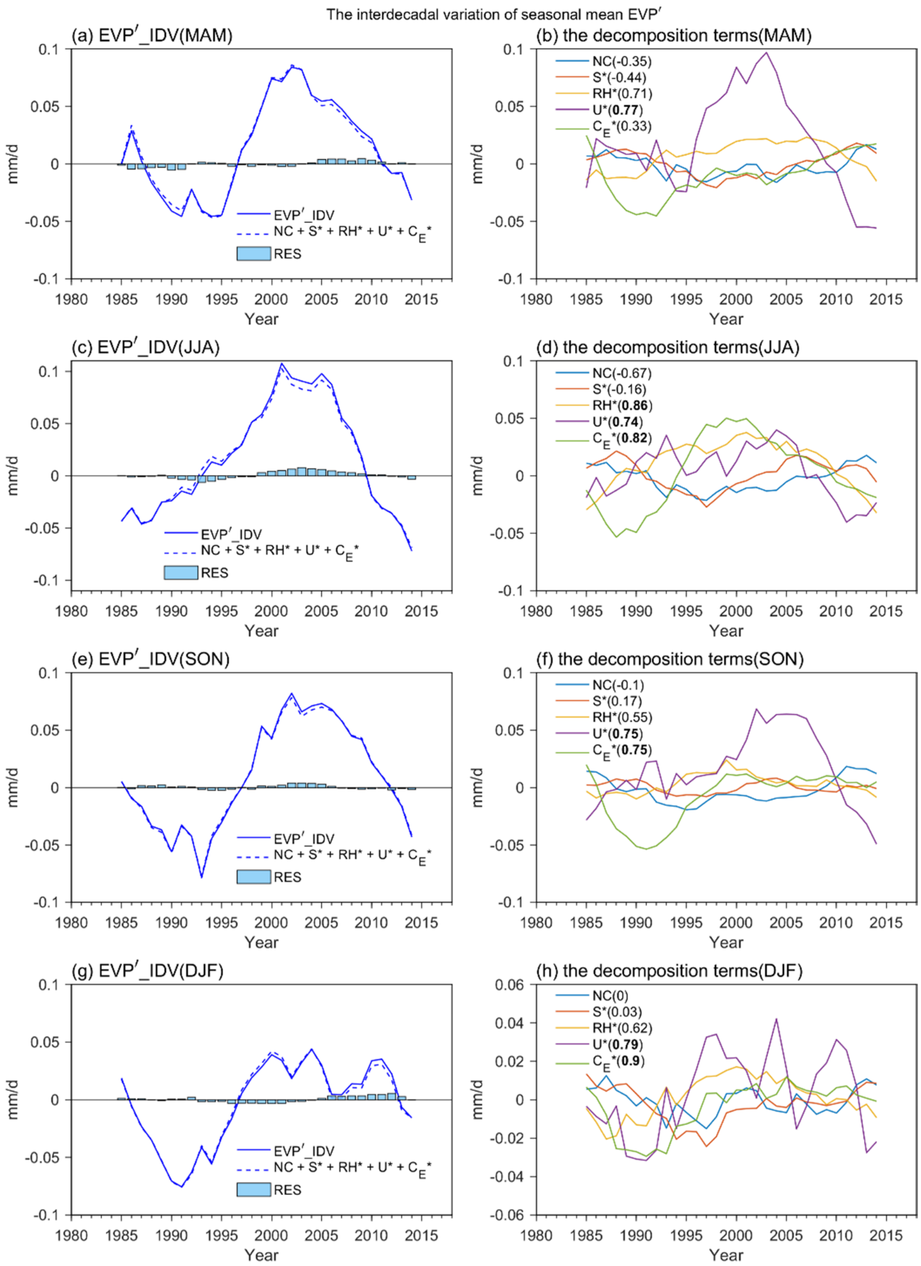

Figure 4. As in Figure 3, for (**a**,**b**) MAM, (**c**,**d**) JJA, (**e**,**f**) SON, and (**g**,**h**) DJF.

To investigate the impacts of climate modes on the IDV of EVP′, we calculated the correlation between the IDVs of major climate modes (PDO, AMO, and NAO) and the annual mean EVP′ and the related decomposition terms (Figure 5). The correlations between the IDV of RH*, U*, and AMO were 0.88 and 0.89 (above the 95% confidence level), respectively. The results indicate that the AMO contributed to the increased EVP′ in the

1990s and the decreased EVP′ after the early 2000s by affecting the RH* and U* (Figure 5a). The correlation between the IDV of C_E* and NAO was −0.8 (above the 95% confidence level), suggesting that the NAO contributed to the decreased EVP′ in the 1980s and the increased EVP′ in the 1990s by affecting the C_E* (Figure 5b). The correlation between the IDVs of EVP′ and PDO was −0.76, which was significant with the 95% confidence level. However, the IDVs of other terms were not significantly correlated with the IDV of PDO (Figure 5d). The 9-year running correlation between the IDVs of U* and PDO was comparable to that of the IDVs of RH*, U*, and AMO in the 1990s, but showed a shape decrease after the early 2000s (Figure 5c). The results indicate that the PDO contributed to the increased EVP′ in the 1990s by affecting the U*. Therefore, the NAO plays an important role in the decreased EVP′ in the 1980s and the increased EVP′ in the 1990s, and the AMO played an important role in the increased EVP′ in the 1990s and the decreased EVP′ after the early 2000s. In addition, the PDO may have an important influence on the IDV of EVP′ by affecting the U* in the 1990s.

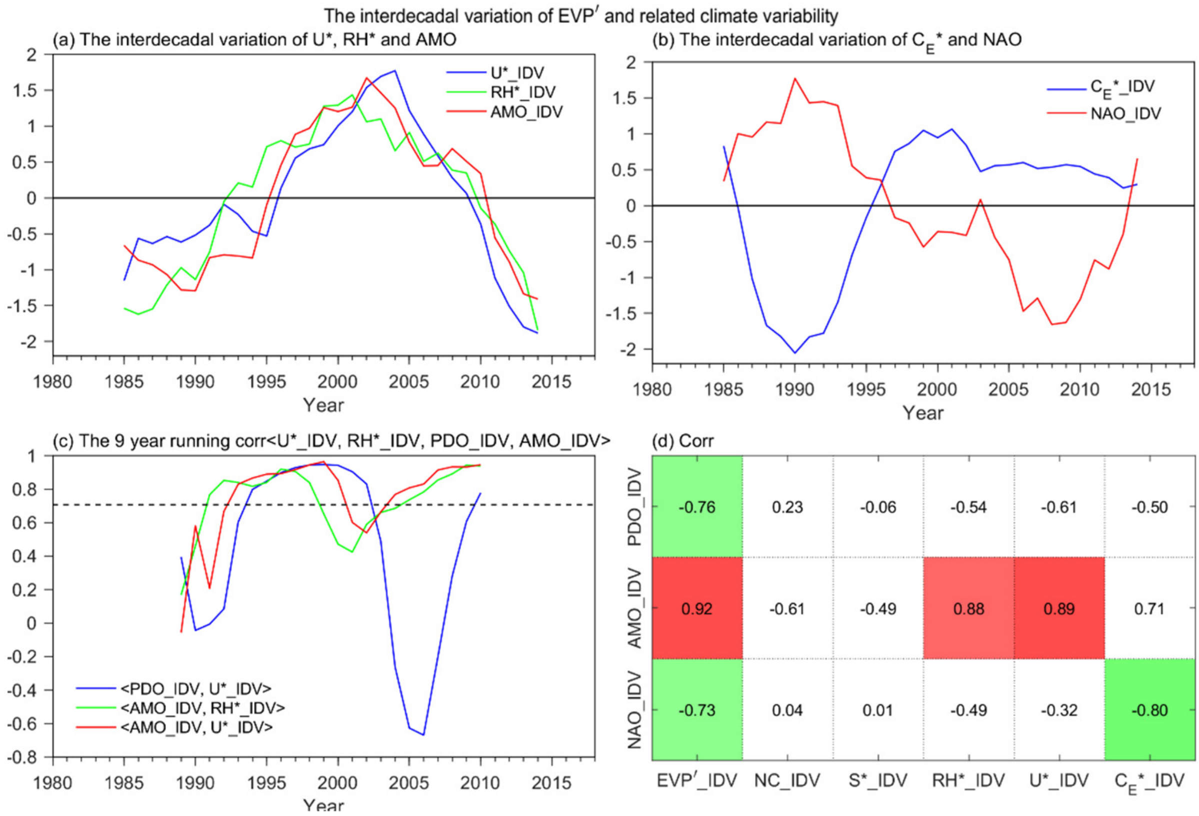

Figure 5. (**a**) The normalized interdecadal variations of U*, PDO, and AMO. (**b**) The normalized interdecadal variations of C_E* and NAO. (**c**) The 9 year running correlations between the interdecadal variations of U* and PDO (the values are multiplied by −1), RH* and AMO, U* and AMO. The black dashed line indicates the 95% confidence level. (**d**) Correlations between the interdecadal variation of PDO, AMO, NAO, and EVP′, NC, S*, RH*, U*, C_E* over the tropical Indian Ocean. The colors indicate significance with the 95% confidence level (the red and green colors indicate positive and negative correlation coefficients, respectively).

4. Conclusions and Discussion

This study focuses on the trend and interdecadal variation of evaporation in the tropical Indian Ocean. The results show that the RH* plays a slightly more important role in the trend of annual mean EVP′. Gao et al. [16] emphasized the important role of humidity difference in the latent heat flux trends. Li et al. [15] suggested that the increasing trend of latent heat flux is strongly associated with the SST warming and strengthening

U during 1977–2006. The IDV of annual mean EVP′ is mainly affected by the U and C_E. Previous studies pointed out that the U plays the important role in the IDV of EVP′ [22,31]. The Atlantic warming induces the wind anomalies over the Indo-western Pacific [35]. The PDO may induce wind anomalies to change the subsurface ocean heat content in the Indian Ocean by the atmospheric bridge [36]. Robertson et al. [25] showed that the variations of C_E* are smaller than the other terms in global ocean evaporation. Morioka et al. [37] suggested that the C_E* contributes to the EVP′ over the south Indian Ocean in December, corresponding to the result of the IDV of EVP′ in DJF. In addition, the C_E* may be affected by the U [26].

In this study, we investigated the trend and interdecadal variation of evaporation over the tropical Indian Ocean in ERA5 for the period of 1980–2018 by the evaporation decomposition method. A significant increasing trend appeared from 1980 to 2018, with a linear trend of 0.083 mm/d/decade. The key terms controlling the increasing trend of annual mean EVP′ were the NC, RH*, and U*, with the linear trends of 0.026, 0.032, and 0.026 mm/d/decade, respectively. The result indicates that the increasing trend of EVP′ was associated with the SST warming and the increasing U*. The decomposition analysis of seasonal mean EVP′ indicates that the C_E* significantly affected the magnitude of the increasing trend of EVP′ in SON.

The IDV of annual mean EVP′ showed a decrease in the 1980s, an increase from the 1990s to the early 2000s, and a decrease from the early 2000s onwards. The decreased EVP′ in the 1980s was attributed to the C_E, the increased EVP′ from the 1990s to the early 2000s, and the decreased EVP′ from the early 2000s onwards were associated with the U. For the IDV of seasonal mean EVP′, the U was the important factor in the IDV of EVP′ in all seasons. The RH* played a key role in the IDV of EVP′ in JJA and the C_E* had an important influence on the IDV of EVP′ in JJA, SON, and DJF. Furthermore, the IDV of the annual mean EVP′ was significantly correlated with the PDO, AMO, and NAO. The AMO contributed to the increased EVP′ in the 1990s and the decreased EVP′ after the early 2000s by affecting the RH* and U*. The NAO contributed to the decreased EVP′ in the 1980s by affecting the C_E*. The PDO may affect the increased EVP′ in the 1990s by the U*.

Author Contributions: Conceptualization, T.S.; methodology, T.S. and B.H.; data curation, T.S. and Z.Z.; writing—original draft preparation, B.H. and Y.W.; writing—review and editing, G.F. and Y.W.; visualization, B.H.; supervision, Z.Z. All authors have read and agreed to the published version of the manuscript.

Funding: This research was funded by the National Natural Science Foundation of China (No.42130610, 41975062, 42175071, 41875097) and the National Key Research and Development Program of China (No.2018YFE0109600).

Institutional Review Board Statement: Not applicable.

Informed Consent Statement: Not applicable.

Data Availability Statement: The ERA5 dataset is available from https://cds.climate.copernicus.eu/cdsapp#!/dataset/reanalysis-era5-single-levels-monthly-means?tab=overview (accessed on 9 January 2022). The ERSSTv5 dataset is available from https://psl.noaa.gov/data/gridded/data.noaa.ersst.v5.html (accessed on 9 January 2022). The PDO, AMO, and NAO are available from http://climexp.knmi.nl/start.cgi?id=bcee887e86deb1c07a57312897c67387 (accessed on 9 January 2022).

Conflicts of Interest: The authors declare no conflict of interest.

References

1. Trenberth, K.E.; Caron, J.M.; Stepaniak, D.P. The atmospheric energy budget and implications for surface fluxes and ocean heat transports. *Clim. Dyn.* **2001**, *17*, 259–276. [CrossRef]
2. Valdivieso, M.; Haines, K.; Balmaseda, M.; Chang, Y.-S.; Drevillon, M.; Ferry, N.; Fujii, Y.; Köhl, A.; Storto, A.; Toyoda, T.; et al. An assessment of air–sea heat fluxes from ocean and coupled reanalyses. *Clim. Dyn.* **2017**, *49*, 983–1008. [CrossRef]
3. Kumar, B.P.; Cronin, M.F.; Joseph, S.; Ravichandran, M.; Sureshkumar, N. Latent Heat Flux Sensitivity to Sea Surface Temperature: Regional Perspectives. *J. Clim.* **2017**, *30*, 129–143. [CrossRef]

4. Wang, C.; Weisberg, R.H.; Yang, H. Effects of the Wind Speed–Evaporation–SST Feedback on the El Niño–Southern Oscillation. *J. Atmos. Sci.* **1999**, *56*, 1391–1403. [CrossRef]
5. Yu, L.; Jin, X.; Josey, S.A.; Lee, T.; Kumar, A.; Wen, C.; Xue, Y. The global ocean water cycle in atmospheric reanalysis, satellite, and ocean salinity. *J. Clim.* **2017**, *30*, 3829–3852. [CrossRef]
6. Cayan, D.R. Latent and Sensible Heat Flux Anomalies over the Northern Oceans: Driving the Sea Surface Temperature. *J. Phys. Oceanogr.* **1992**, *22*, 859–881. [CrossRef]
7. Alory, G.; Wijffels, S.; Meyers, G. Observed temperature trends in the Indian Ocean over 1960–1999 and associated mechanisms. *Geophys. Res. Lett.* **2007**, *34*, L02606. [CrossRef]
8. Du, Y.; Xie, S.-P. Role of atmospheric adjustments in the tropical Indian Ocean warming during the 20th century in climate models. *Geophys. Res. Lett.* **2008**, *35*, L08712. [CrossRef]
9. Chen, X.; Yao, Y.; Zhao, S.; Li, Y.; Jia, K.; Zhang, X.; Shang, K.; Xu, J.; Bei, X. Estimation of High-Resolution Global Monthly Ocean Latent Heat Flux from MODIS SST Product and AMSR-E Data. *Adv. Meteorol.* **2020**, *2020*. [CrossRef]
10. Zeng, L.; Shi, P.; Liu, W.T.; Wang, D. Evaluation of a satellite-derived latent heat flux product in the South China Sea: A comparison with moored buoy data and various products. *Atmos. Res.* **2009**, *94*, 91–105. [CrossRef]
11. Bourras, D. Comparison of Five Satellite-Derived Latent Heat Flux Products to Moored Buoy Data. *J. Clim.* **2006**, *19*, 6291–6313. [CrossRef]
12. Hegerl, G.C.; Black, E.; Allan, R.P.; Ingram, W.J.; Polson, D.; Trenberth, K.E.; Chadwick, R.S.; Arkin, P.A.; Sarojini, B.B.; Becker, A.; et al. Challenges in Quantifying Changes in the Global Water Cycle. *Bull. Am. Meteorol. Soc.* **2015**, *96*, 1097–1115. [CrossRef]
13. Kang, S.; Ahn, J.-B. Global energy and water balances in the latest reanalyses. *Asia-Pac. J. Atmos. Sci.* **2015**, *51*, 293–302. [CrossRef]
14. Liu, J.; Curry, J.A. Variability of the tropical and subtropical ocean surface latent heat flux during 1989–2000. *Geophys. Res. Lett.* **2006**, *33*, L05706. [CrossRef]
15. Li, G.; Ren, B.; Yang, C.; Zheng, J. Revisiting the trend of the tropical and subtropical Pacific surface latent heat flux during 1977–2006. *J. Geophys. Res. Atmos.* **2011**, *116*, D10115. [CrossRef]
16. Gao, S.; Chiu, L.S.; Shie, C.-L. Trends and variations of ocean surface latent heat flux: Results from GSSTF2c data set. *Geophys. Res. Lett.* **2013**, *40*, 380–385. [CrossRef]
17. Pokhrel, S.; Dutta, U.; Rahaman, H.; Chaudhari, H.; Hazra, A.; Saha, S.K.; Veeranjaneyulu, C. Evaluation of Different Heat Flux Products Over the Tropical Indian Ocean. *Earth Space Sci.* **2020**, *7*, e2019EA000988. [CrossRef]
18. Liu, W.T.; Katsaros, K.B.; Businger, J.A. Bulk Parameterization of Air-Sea Exchanges of Heat and Water Vapor Including the Molecular Constraints at the Interface. *J. Atmos. Sci.* **1979**, *36*, 1722–1735. [CrossRef]
19. Richter, I.; Xie, S.-P. Muted precipitation increase in global warming simulations: A surface evaporation perspective. *J. Geophys. Res.* **2008**, *113*, D24118. [CrossRef]
20. Wu, R.; Kirtman, B.P.; Pegion, K. Local Air–Sea Relationship in Observations and Model Simulations. *J. Clim.* **2006**, *19*, 4914–4932. [CrossRef]
21. Lorenz, D.J.; DeWeaver, E.T.; Vimont, D.J. Evaporation Change and Global Warming: The Role of Net Radiation and Relative Humidity. *J. Geophys. Res.* **2010**, *115*, D20118. [CrossRef]
22. Yu, L. Global Variations in Oceanic Evaporation (1958–2005): The Role of the Changing Wind Speed. *J. Clim.* **2007**, *20*, 5376–5390. [CrossRef]
23. Xie, S.-P.; Philander, S.G.H. A coupled ocean-atmosphere model of relevance to the ITCZ in the eastern Pacific. *Tellus A* **1994**, *46*, 340–350. [CrossRef]
24. Zhou, X.; Ray, P.; Barrett, B.S.; Hsu, P.-C. Understanding the bias in surface latent and sensible heat fluxes in contemporary AGCMs over tropical oceans. *Clim. Dyn.* **2020**, *55*, 2957–2978. [CrossRef]
25. Robertson, F.R.; Bosilovich, M.G.; Roberts, J.B.; Reichle, R.H.; Adler, R.; Ricciardulli, L.; Berg, W.; Huffman, G.J. Consistency of Estimated Global Water Cycle Variations over the Satellite Era. *J. Clim.* **2014**, *27*, 6135–6154. [CrossRef]
26. Bosilovich, M.G.; Robertson, F.R.; Takacs, L.; Molod, A.; Mocko, D. Atmospheric Water Balance and Variability in the MERRA-2 Reanalysis. *J. Clim.* **2017**, *30*, 1177–1196. [CrossRef]
27. Hersbach, H.; Bell, B.; Berrisford, P.; Hirahara, S.; Horányi, A.; Muñoz-Sabater, J.; Nicolas, J.; Peubey, C.; Radu, R.; Schepers, D.; et al. The ERA5 global reanalysis. *Q. J. R. Meteorol. Soc.* **2020**, *146*, 1999–2049. [CrossRef]
28. Huang, B.; Thorne, P.W.; Banzon, V.F.; Boyer, T.; Chepurin, G.; Lawrimore, J.H.; Menne, M.J.; Smith, T.M.; Vose, R.S.; Zhang, H.-M. Extended Reconstructed Sea Surface Temperature, Version 5 (ERSSTv5): Upgrades, Validations, and Intercomparisons. *J. Clim.* **2017**, *30*, 8179–8205. [CrossRef]
29. Pyper, B.J.; Peterman, R.M. Comparison of methods to account for autocorrelation in correlation analyses of fish data. *Can. J. Fish. Aquat. Sci.* **1998**, *55*, 2127–2140. [CrossRef]
30. Li, J.; Sun, C.; Jin, F.F. NAO implicated as a predictor of Northern Hemisphere mean temperature multidecadal variability. *Geophys. Res. Lett.* **2013**, *40*, 5497–5502. [CrossRef]
31. Cao, N.; Ren, B. Regime shift of global oceanic evaporation in the late 1990s using OAFlux dataset. *Theor. Appl. Climatol.* **2019**, *136*, 1407–1417. [CrossRef]
32. Tao, W.; Huang, G.; Hu, K.; Qu, X.; Wen, G.; Gong, H. Interdecadal modulation of ENSO teleconnections to the Indian Ocean Basin Mode and their relationship under global warming in CMIP5 models. *Int. J. Climatol.* **2015**, *35*, 391–407. [CrossRef]

33. Young, I.R.; Zieger, S.; Babanin, A.V. Global trends in wind speed and wave height. *Science* **2011**, *332*, 451–455. [CrossRef] [PubMed]
34. Li, G.; Ren, B. Evidence for strengthening of the tropical Pacific Ocean surface wind speed during 1979–2001. *Theor. Appl. Climatol.* **2012**, *107*, 59–72. [CrossRef]
35. Li, X.; Xie, S.P.; Gille, S.T.; Yoo, C. Atlantic-induced pan-tropical climate change over the past three decades. *Nat. Clim. Chang.* **2016**, *6*, 275–279. [CrossRef]
36. Jin, X.; Kwon, Y.O.; Ummenhofer, C.C.; Seo, H.; Schwarzkopf, F.U.; Biastoch, A.; Böning, C.W.; Wright, J.S. Influences of pacific climate variability on decadal subsurface Ocean heat content variations in the Indian Ocean. *J. Clim.* **2018**, *31*, 4157–4174. [CrossRef]
37. Morioka, Y.; Tozuka, T.; Masson, S.; Terray, P.; Luo, J.-J.; Yamagata, T. Subtropical Dipole Modes Simulated in a Coupled General Circulation Model. *J. Clim.* **2012**, *25*, 4029–4047. [CrossRef]